Influence of Three-Dimensional Radiative Effects on the Spatial Distribution of Shortwave Cloud Reflection

TAMÁS VÁRNAI*

Department of Atmospheric and Oceanic Sciences, McGill University, Montreal, Quebec, Canada

(Manuscript received 3 February 1998, in final form 1 December 1998)

ABSTRACT

This paper examines how three-dimensional radiative effects influence the way cloud fields appear in high-resolution shortwave satellite images. To do so, it uses cloud reflectance fields simulated by a Monte Carlo radiative transfer model. This study examines the influence of the two counteracting three-dimensional mechanisms: the smoothing effect of radiative diffusion, which can reduce brightness variations, and the sharpening effect caused by thick areas intercepting extra radiation through their sides and casting shadows on the thin areas behind them, which can enhance brightness variability. The findings suggest that current high-resolution retrievals of cloud structure can be significantly biased because they do not take these effects into account. For oblique sun, high-resolution retrievals can overestimate both the scene-averaged optical thickness and the magnitude of cloud variability, and yield systematically distorted cloud shapes and artificially anisotropic cloud structures. It is shown that the biases are especially large when cloud-top height variations are present because cloud-top variations can cause a much stronger sharpening effect than internal cloud variability. To prevent erroneous interpretation of retrieval results, an algorithm is proposed to determine whether retrievals based on any satellite image are affected significantly by these biases.

1. Introduction

Satellite measurements of cloud reflectivity are often used to retrieve various cloud properties such as optical thickness, liquid water content, effective radius, albedo, and cloud-top height (CTH). However, numerous studies have pointed out that solar reflectivities at any given point are not fully determined by local cloud properties but are also influenced by interactions among nearby cloud elements (Davies 1976; McKee and Klehr 1978; Barker and Davies 1992b; Cahalan et al. 1994; Barker and Liu 1995). It is therefore important to examine the relationship between the spatial distribution of cloud properties and the structure of reflectivity fields.

Many previous studies have investigated the way cloud heterogeneities—most importantly, cloud optical thickness variations—influence the spatial distribution of reflected radiance. Most of these papers focused on the effects of optical thickness variations that were due to horizontal changes in the volume extinction coefficient and assumed flat cloud tops. These studies found that since radiative interactions among nearby cloud elements tend to smooth out the differences among their reflectivities, radiance fields tend to be smoother than optical thickness fields (Stephens 1988; Evans 1993; Gabriel et al. 1993; Marshak et al. 1995a,b; Davis et al. 1997; Chambers et al. 1997).

Lidar measurements (e.g., Boers et al. 1988) and everyday experience both indicate that the distribution of cloud optical thickness is also largely influenced by variations in the cloud-top height. Recent studies by Várnai (1996), Loeb et al. (1997, 1998), Loeb and Coakley (1998), and Várnai and Davies (1999) have shown that CTH variations have very different—usually stronger—effects on scene-average reflectivity than volume extinction coefficient variations do. Davies (1976) and Zuidema and Evans (1998) pointed out that for CTH variations, two-dimensional radiative interactions (taking place in the solar plane) can counteract the smoothing effects observed in previous studies, and enhance the brightness differences between nearby pixels. The main purpose of this paper is to examine the effects of CTH variations on the spatial distribution of cloud reflectivity in three dimensions and to compare these effects to the influence of horizontal volume extinction coefficient variations.

Since examining such effects requires extremely lengthy radiative transfer calculations, this paper examines only one cloud field. While individual case stud-

* Current affiliation: University of Maryland, Baltimore County, Baltimore, Maryland.

Corresponding author address: Dr. Tamás Várnai, Climate and Radiation Branch, Code 913, NASA Goddard Space Flight Center, Greenbelt, MD 20771.
E-mail: varnai@climate.gsfc.nasa.gov

© 2000 American Meteorological Society

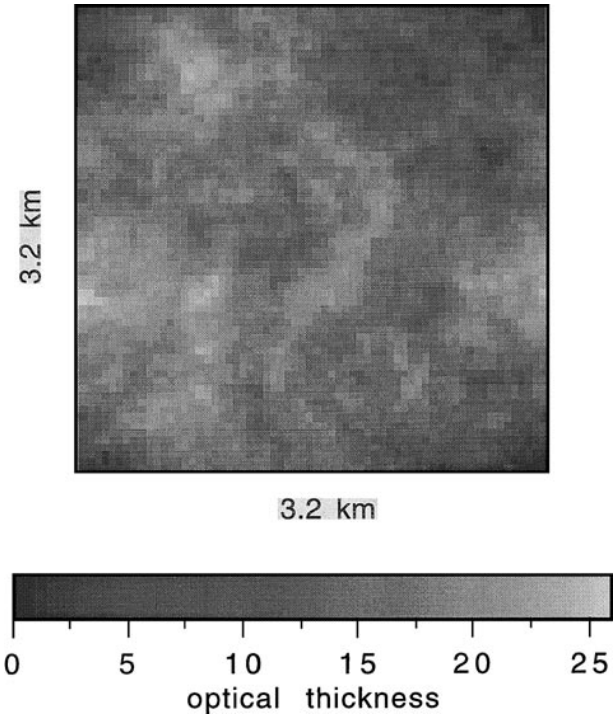

FIG. 1. Optical thickness field of the simulated scene.

ies inherently cannot estimate the radiative influence of cloud heterogeneities on a globally representative distribution of cloud types, they can be valuable in pointing out some previously unexplored phenomena. The present study examines a scene that can be regarded as representative of cumulus clouds with moderate cloud variability.

The structure of this paper is as follows. First, section 2 describes the experimental setup, and then sections 3, 4, and 5 analyze the results. Section 3 examines the frequency distributions of individual pixel reflectances; section 4 discusses the spatial distributions of cloud reflection; and section 5 analyzes how various cloud and illumination characteristics influence radiative interactions among nearby areas. Finally, section 6 offers a brief summary and a few concluding remarks.

2. Experiment description

This paper examines the solar reflection of a scene whose horizontal optical thickness distribution was generated by the stochastic cloud model described in Barker and Davies (1992a). This scene is shown in Fig. 1, and its main parameters are listed in Table 1. While this scene is not a true cloud field, it is believed to reproduce the most important features of real cloud variability. The main advantage of using a stochastic model over retrieving the optical thickness field from measurements is that stochastic models can result in periodic cloud fields. The importance of this periodicity can be illustrated through the following argument.

TABLE 1. Main parameters of the cloud field used for the Monte Carlo simulations.

Scene size	$(3.2\ \mathrm{km})^2$
Horizontal resolution	50 m
Cloud fraction	1
Average optical depth	15
Minimum optical depth	1
Maximum optical depth	26
Scaling parameter s*	−2.85

* See Barker and Davies (1992a) for definition.

Ideally, one should simulate radiative transfer through large scenes so that the artificial effects at the scene edge do not significantly contaminate the results. Unfortunately, since the computational requirements of radiative transfer calculations increase rapidly with scene size, it is currently impossible to perform detailed radiative transfer calculations for large scenes. This problem is usually solved by taking a small scene and building large ''virtual scenes'' by repeating the same small scene infinitely in all directions. (In practice, this is done by simulating radiative transfer over the small scene and by assuming that the radiation, which leaves at one edge of this scene, instantly comes back at the opposite edge.) However, if the small scene is not periodic, the large ''virtual'' scene will have unrealistic, abrupt changes at the edges of neighboring small scenes—an artifact that can be avoided only by using periodic small scenes.

In this study, cloud reflection is calculated using the Monte Carlo radiative transfer model described in Várnai (1996). The model assumes a single scattering albedo of 1.0 and uses a Mie scattering phase function that is representative of the $\mathrm{Sc}_{\mathrm{top}}$ drop size distribution of Welch et al. (1980) at 0.865-μm wavelength. Since Rayleigh scattering is negligible at this wavelength, and there is usually little aerosol above the cloud top (where it could influence the spatial distribution of cloud reflection the most), the effects of surrounding air are not considered. Reflection by the underlying surface is also ignored, which makes the results most representative of clouds over dark surfaces such as oceans.

Three separate simulations are performed for the optical thickness field shown in Fig. 1. The first one uses the independent pixel approximation (IPA) (Cahalan et al. 1994) to calculate cloud reflection by simulating three-dimensional radiative transfer but assuming that, instead of $(50\ \mathrm{m})^2$, each pixel covers areas of $(100\ \mathrm{km})^2$. This enlargement reduces the number of photons moving from one pixel to another, thus resulting in pixels whose reflection is essentially independent from their surroundings. Following most previous studies, the second simulation assumes the geometrical cloud thickness to be constant and attributes all optical thickness variations to changes in the volume extinction coefficient. Finally, the third simulation assumes a constant cloud volume extinction coefficient (VEC) and attributes all optical thickness variations to changes in CTH.

To make the comparison of these three representations

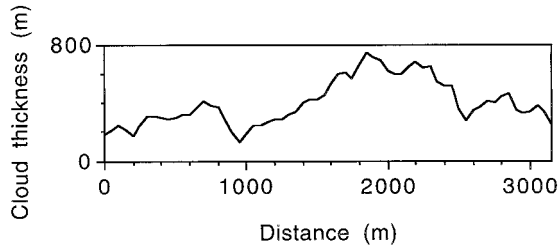

FIG. 2. Geometrical cloud thickness variations along column 55 of the scene in Fig. 1.

of cloud heterogeneities most appropriate, this study assumes the same average cloud geometrical thickness (0.5 km) and VEC (30 km^{-1}) values in all three simulations. [This is important because cloud radiative properties change with the geometrical cloud thickness and volume extinction coefficient (Barker and Liu 1995).] Figure 2 shows the vertical cross section of CTH variations along column 55. The variations in this column can be regarded as representative of the entire field since the standard deviation of optical thickness (τ) values in this column (4.71) is close to the average standard deviation of all columns (4.24). The 4.24 standard deviation of the entire optical thickness field can be considered realistic since it lies in the range ($3.3 < \sigma < 5.4$) observed by Loeb et al. (1998).

The Monte Carlo experiments yield the horizontal distribution of bidirectional reflectance factor (BRF) or reflectance, defined as

$$\mathrm{BRF}_{(x,y,\theta,\varphi)} = \frac{\pi I_{(x,y,\theta,\varphi)}}{\mu_0 S_0}.$$

In this equation, x and y are the horizontal coordinates, θ and φ are the viewing zenith and azimuth angles, and I is the reflected radiance; μ_0 indicates the cosine of the solar zenith angle and S_0, the solar irradiance. The solar zenith angle is set to 60°, and three viewing angles are considered: overhead view, and 50° viewing zenith angles in the forward and backscatter directions. As an example, Fig. 3 shows the reflectance fields obtained for the three view directions in the case of CTH variations.

The Monte Carlo model estimates the reflectance values based on the flux reflected into directions that are within 10° of the nominal view direction. As a result, the model assumes that the ratio of the reflectance in the nominal view direction to the flux going into a 10° wide angular bin is constant throughout the entire scene. The errors due to this assumption were estimated by comparing the results to values obtained from the same simulation but allowing for a 15° difference between the photon's direction and the nominal view angle. The examination revealed that the assumption introduced errors of less than 0.001 and 0.01 into the individual pixel reflectances obtained for 0° and 50° viewing zenith angles, respectively, and that it had negligible effects on

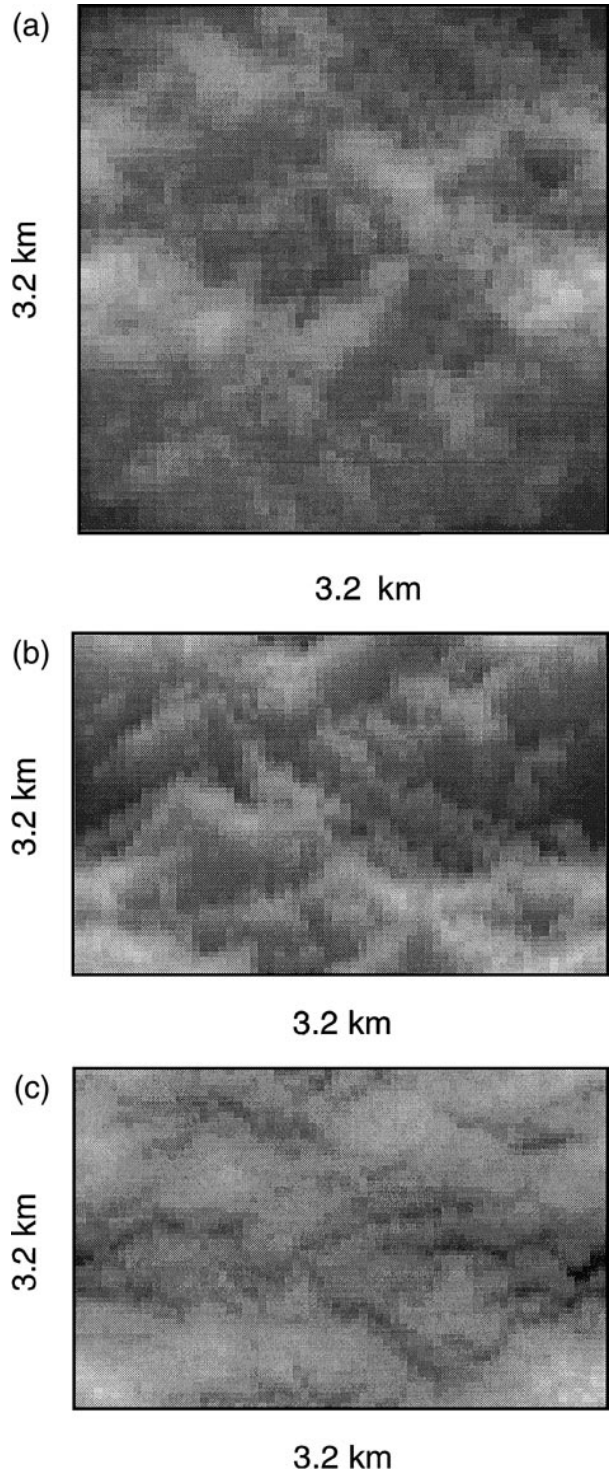

FIG. 3. Reflectance fields calculated for the scene in Fig. 1, assuming CTH variations. (a) Top view (the sun is shining from the top side of the image); (b) and (c) views from the forward and backscattering directions, respectively.

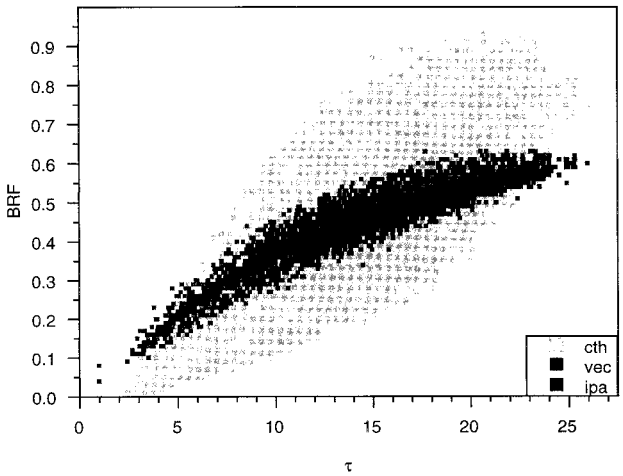

FIG. 4. Relationship between nadir reflectance and optical thickness in the three Monte Carlo simulations.

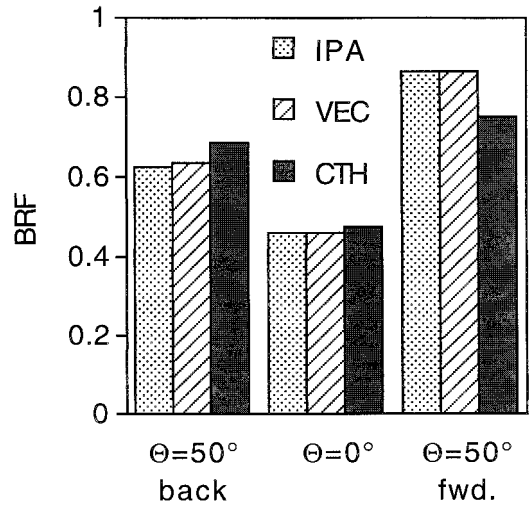

FIG. 5. Scene average of simulated reflectances for the scene in Fig. 1.

the statistical parameters of the reflectance fields (average, standard deviation, skewness, and scaling parameter). Since each simulation used 8×10^8 photons, the statistical uncertainty of individual pixel reflectances is usually less than 0.01, and has no significant effect on the reflectance field parameters.

3. Frequency distribution of individual pixel reflection

a. Reflectance

This section discusses the first three moments (average, standard deviation, and skewness) of the reflectance fields obtained through Monte Carlo simulations.

Examining the scene-averaged reflectances reveals systematic differences for the three simulations (Figure 5). In agreement with the findings of many previous studies (Davies 1984; Kobayashi 1993), three-dimensional effects (not present in the IPA) reduce forward scattering and enhance reflection to the backscatter direction. As in Loeb et al. (1998), these effects are stronger for CTH than for volume extinction VEC variations.

Turning now to the reflectances of individual pixels, we can see in Fig. 4 that in the IPA, the optical thickness fully determines the reflectance (the slight scatter is due to the Monte Carlo noise). However, the figure also shows that for volume extinction coefficient variations there is no one-to-one relationship between optical thickness and reflectance [as Barker and Davies (1992b), Cahalan et al (1994), and Barker and Liu (1995) reported], and that this relationship is even weaker for CTH variations. This implies that horizontal photon transport (i.e., radiative interaction among nearby pixels) influences not only the scene-average reflectance but also the individual pixel reflectances, much more for CTH than VEC variations. Consequently, satellite retrievals of cloud optical thickness (that use the IPA) cannot only have stronger overall biases where CTH variations exist but can also yield patterns that are further away from the true patterns of τ-variations.

Figure 4 also points out that (especially for CTH variations) three-dimensional interactions tend to reduce the brightness of the thinnest pixels and to enhance the brightness of the thickest ones. This can be explained by considering that [as described by Davies (1976, p. 139) and Zuidema and Evans (1998)] the thinnest pixels are often in the shadow of thicker ones and that the thickest pixels get extra illumination through their sides. The result of this tendency is that, although horizontal photon transport reduces small-scale reflectance variations, it actually increases the overall variability of the reflectance field by increasing the magnitude of the larger scale variations (Fig. 6). The increase is greatest for the forward view, in which both sunlit and shadowed areas are visible, and the sunlit areas are very bright

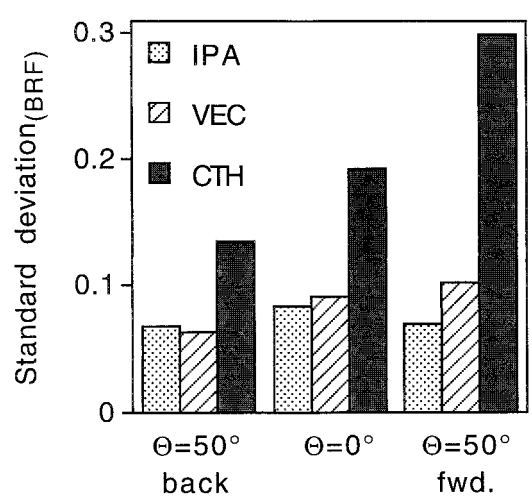

FIG. 6. Standard deviation of simulated reflectances for the scene in Fig. 1.

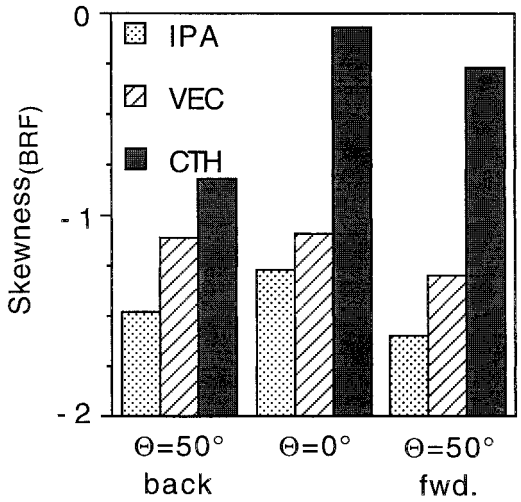

FIG. 7. Skewness of simulated reflectances for the scene in Fig. 1.

due to the forward peak in cloud reflection. In contrast, since nadir reflection is not so large even for the sunlit areas, the standard deviation is smaller for the nadir view. The standard deviation is smallest for the backscatter view since from this direction, mostly sunlit pixels are visible and the shadowed areas are almost completely obscured (Fig. 3c).

After the first two moments (the $\overline{\mathrm{BRF}}$ mean and the σ standard deviation), the third moment (the skewness) of the frequency distribution of reflectances can also be examined. The skewness (γ), defined as

$$\gamma = \frac{1}{N_{\mathrm{pixel}}\sigma^3} \sum_{n=1}^{N_{\mathrm{pixel}}} (\mathrm{BRF}_n - \overline{\mathrm{BRF}})^3,$$

describes whether the frequency distribution is symmetric over the mean value. A positive skewness indicates that the frequency distribution has a larger tail toward high values and a negative skewness that the tail is larger toward small values. If the cloud generation model created many cloud fields, their average skewness would be zero. However, the random nature of the generation process resulted in a skewness equal to -0.36 for the τ-field in Fig. 1. This value is close to the -0.375 average skewness of CTH variations observed by Boers et al. (1988).

The skewness of the reflectances calculated using the IPA is significantly more negative (-1.267, -1.604, and -1.482 for the nadir, forward scatter, and backscatter views, respectively) than the skewness of the original τ-field. This decrease is caused by the nonlinearity of the $\mathrm{BRF}_{(\tau)}$ function (see the IPA results in Fig. 4): the frequency distribution's tail toward higher values gets compressed when the τ-values are transformed to reflectances because for thick clouds, the reflectance hardly increases with τ. In comparison, the tail toward small values gets elongated because for thin clouds, the reflectance changes quickly with optical thickness.

As Fig. 7 shows, horizontal photon transport increases the skewness of the reflectance field significantly, especially for CTH variations. The increase is caused by many pixels at the sunlit slopes being brightened by the extra illumination they receive through their sides. These pixels enlarge the frequency distribution's tail that reaches toward high values and hence increase the skewness, resulting in less negative values.

b. Retrieved optical thickness

Since reflectance values observed by satellites are often used to retrieve cloud optical thickness, it is of interest to examine the effects of the above tendencies on the distribution of retrieved optical thickness values. As in all current satellite retrieval methods, the IPA is used to transform the simulated reflectance values to optical thicknesses.

For large reflectances, even small Monte Carlo errors in the reflectance values can cause large deviations in the retrieved optical thicknesses. Due to the nonlinearity of the $\mathrm{BRF}_{(\tau)}$ function, these errors can increase the mean, standard deviation, and skewness values of the retrieved optical thickness field. To avoid this problem, the maximum retrieved optical thickness is set to 60. This limit affects 8% to 13% of the pixels in the CTH fields but does not affect any pixels in the VEC and IPA fields. Since the limit influences so many pixels, it is likely to overcompensate for the effects of Monte Carlo errors. Thus, the average, standard deviation, and skewness values tend to be underestimated (compared to values retrieved from perfectly exact reflectance fields, if no upper limit is set for the retrieved optical thicknesses). Underestimation is preferable to overestimation since this study points out trends that increase these parameters for the CTH fields, and an underestimation ensures that no artificial trends are created by erroneous overestimations.

If the scene-average reflectance values are used to retrieve the scene-average optical thickness, the estimate is too low (12.8 and 7.5 for VEC and CTH variations, respectively) for the forward view, and too high for the backscatter view (15.6 and 19.0, respectively). If, however, the optical thickness of each pixel is retrieved individually, the scene-averaged optical thickness is overestimated for all viewing directions (Fig. 8). This is in agreement with the findings of Zuidema and Evans (1998), who detected this tendency for the nadir views of numerous observed cloud fields. The tendency is much stronger for CTH than for VEC variations. Though the overestimation is largest for the backscatter view (for which horizontal photon transport increases the scene-average reflectance value), it is clearly present even for the forward view (in which the scene-average reflectance is decreased). The overestimation can be explained by considering that for thick clouds, the IPA reflectance increases slowly with optical thickness (Fig. 4), and as a result, the retrieved optical thickness of the bright pixels at the sunlit cloud sides must be increased

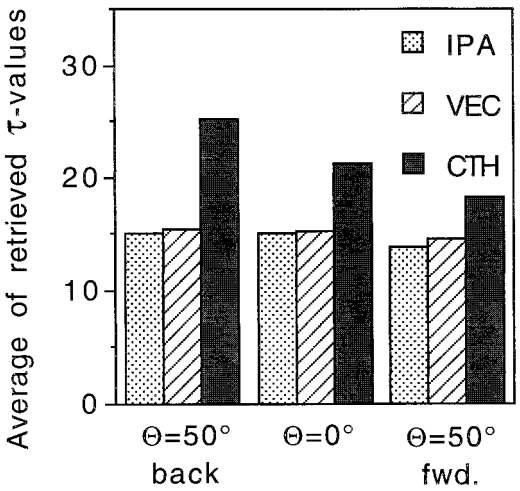

FIG. 8. Scene average of τ-values retrieved at 50-m resolution.

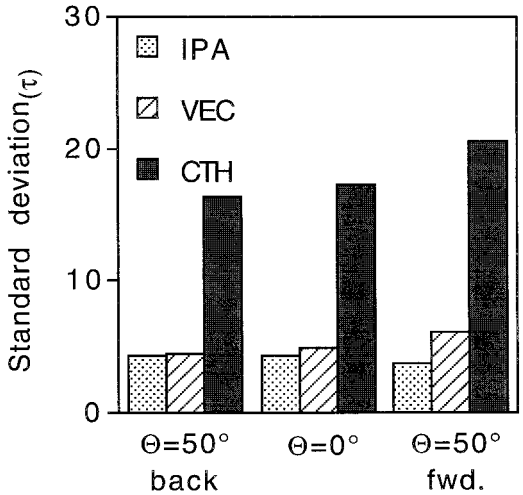

FIG. 9. Standard deviation of the retrieved τ-values.

by large amounts to match the brightening due to side-illumination effects. (The overestimation is probably even stronger for broken cloud fields: since these clouds intercept more incoming solar radiation than is assumed in the IPA, the retrievals must account for the reflection of the extra intercepted radiation by increasing the retrieved optical thickness values.) It should be noted that the overestimation of average optical thickness in high-resolution retrievals is opposite to the underestimation reported by Barker and Liu (1995). The difference is probably due to three-dimensional effects being larger in the present study, both because it uses larger solar zenith angle and average optical thickness values and because (unlike Barker and Liu's study) it includes cloud top height variations, which result in stronger effects than volume extinction coefficient variations.

Having examined the mean of the retrieved optical thicknesses, let us turn to their standard deviation. Like the tendency for reflectances in Fig. 6, the standard deviations of the retrieved optical thicknesses are significantly overestimated, especially for CTH variations (Fig. 9). The overestimation occurs because the retrievals do not compensate for the effects of horizontal photon transport that enhance reflectance variations. The main implication of this overestimation is that on satellite images obtained for oblique sun, scenes that have CTH variations appear to be significantly more heterogeneous than they really are.

Finally, examining the skewness of the retrieved τ-fields reveals a tendency similar to the one in Fig. 7: horizontal photon transport (especially for CTH variations) largely increases the skewness of the retrieved τ-values (Fig. 10). This difference between the true and retrieved skewnesses suggests that one may expect different skewnesses from CTH and optical thickness measurements even when the two variables are well correlated. (One can often expect such a correlation in cases where strong updrafts result in both large optical thickness values and in bumps in the cloud-top surface, while downdrafts cause both lower optical thicknesses and dips in the cloud-top surface.)

4. Spatial distribution of reflectance

While section 3 examined the way three-dimensional radiative effects influence the frequency distribution of individual pixel reflectances, this section focuses on their effects on the spatial patterns of the reflectance field. First, section 3a discusses the differences between the sunlit and shadowy cloud sides; then section 3b examines the Fourier power spectrum of the variations.

a. Differences between sunlit and shadowy cloud sides

For oblique sun, the sunlit cloud sides get more solar illumination than the shadowy ones and hence tend to

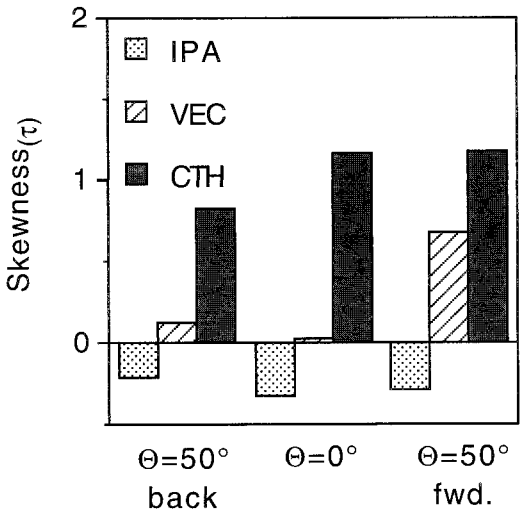

FIG. 10. Skewness of the retrieved τ-values.

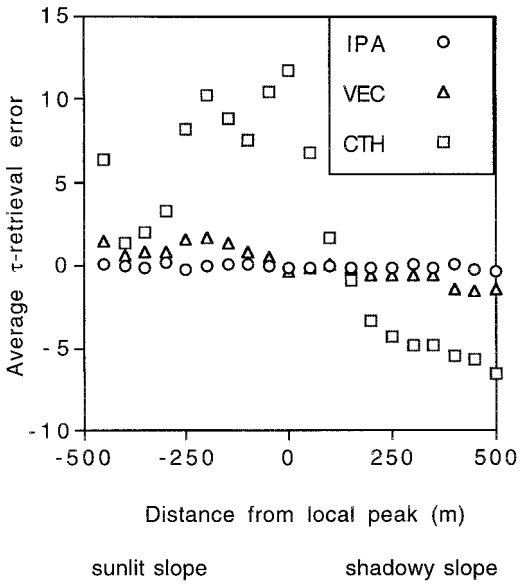

FIG. 11. Average error of optical thickness retrievals on the sunlit and shadowy slopes.

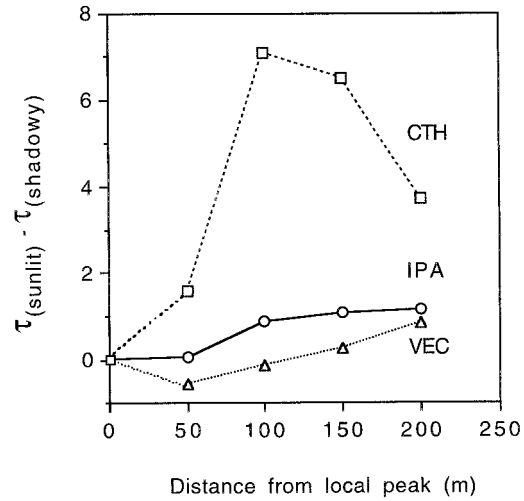

FIG. 12. Average difference between the optical thicknesses retrieved for the sunlit and shadowy slopes.

appear brighter. As a result, it can be expected that optical thickness retrievals yield systematically biased cloud geometries, as if they moved some cloud particles from the shadowy sides to the sunlit slopes. The magnitude of this effect can be illustrated by carrying out the algorithm that follows.

First, the local peaks separating the sunlit and shadowy slopes are selected. These local peaks are defined such that the optical thickness must increase monotonically for at least 100 m in front of them (in the direction parallel to the solar azimuth) and must decrease for at least 100 m behind them. Second, the extent of the sunlit and shadowy slopes is determined by checking where the steady τ-decrease ends as we move farther from the local peak (again, in directions parallel to the solar azimuth). Finally, the scene averages of the pixel-by-pixel τ-retrieval errors are examined as a function of the distance from the local peak.

The results in Fig. 11 reveal no systematic biases if radiation propagates according to the IPA and only small biases for VEC variations. However, the figure also indicates that high-resolution τ-retrievals yield significantly distorted cloud geometries if CTH variations are present. It also shows that optical thicknesses tend to be overestimated even at the beginning of the shadowy sides (near the local peaks), which is probably due to a strong diffusion of light from the sunlit cloud sides.

While the effect described above can distort the retrieved cloud geometries, it may also be used to detect whether the distortion is significant for any particular satellite image. [Note that since the differences between the sunlit and shadowy slopes are caused by the same side-illumination and shadowing effects that change the frequency distribution of the retrieved optical thicknesses (see section 3), finding a large distortion indicates that the frequency distribution of the retrieved τ-values is also biased.] The main steps of such a detection algorithm could be the following: 1) to resample the satellite images in directions parallel and perpendicular to the solar azimuth; 2) to find the local peaks and the cloud slopes; and 3) to compare the averages of optical thicknesses retrieved for the sunlit and shadowy slopes (excluding the pixels that are at the very bottom of the slopes tilted toward the sun since they are often shadowed by clouds in front of them). Figure 12 shows that such an algorithm is capable of clearly indicating that large biases are present for CTH variations, even if—as mentioned above—the maximum retrieved optical thickness is set to 60. Unfortunately, however, this algorithm cannot distinguish the asymmetry caused by radiative effects from the true asymmetry of the cloud field (caused by, for example, a strong wind shear). Therefore, if the real scene is suspected to be asymmetric to the solar azimuth, it may be useful to check whether the thermal infrared image of the same scene shows an asymmetry that can explain the asymmetry of the visible image.

b. Fourier power spectrum

Like many previous papers (Cahalan and Snider 1989; Barker and Davies 1992b; Lovejoy et al. 1993; Pflug and Lovejoy 1993; Tessier et al. 1993; Marshak et al. 1995a,b; Davis et al. 1997; Zuidema and Evans 1998), this study examines the spatial structure of cloud reflection variations using their Fourier power spectrum.

Since the reflectances calculated using the IPA depend only on the optical thickness, their spectrum closely follows the spectrum of optical thickness variations. Figure 13a shows that the two-dimensional spectrum of nadir reflectance is azimuthally symmetric, indicating

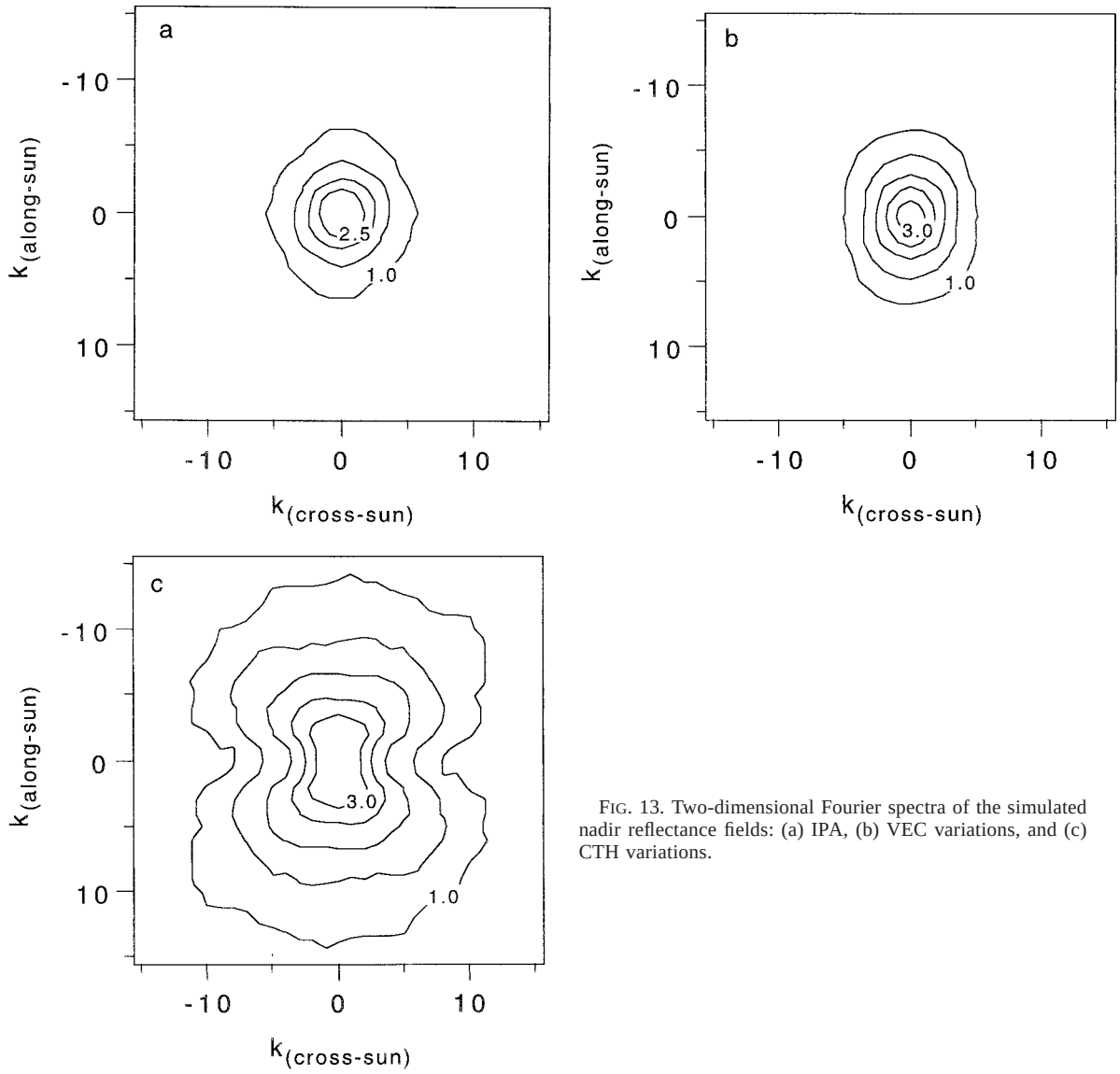

FIG. 13. Two-dimensional Fourier spectra of the simulated nadir reflectance fields: (a) IPA, (b) VEC variations, and (c) CTH variations.

that the variations are statistically similar in directions parallel and perpendicular to the sun. (These two directions can also be referred to as ''along-sun'' and ''cross-sun'' directions.) However, Figs. 13b and 13c indicate significant asymmetries for volume extinction coefficient and CTH variations. The fact that the Fourier power falls off much more quickly in the cross-sun than in the along-sun direction indicates that the reflectance field has much stronger variations in the latter than in the former direction.

The reason for this azimuthal asymmetry can be illustrated through the example of a turreted stratus cloud that has periodic variations in one direction (Fig. 14a). If the sun is perpendicular to the variations, the turrets that cover only half of the cloud field intercept all of the incoming solar radiation. As a result, the turrets are very bright and the shadowed gaps are very dark. If, however, the sun is parallel to the turrets, the incoming radiation reaches both turrets and gaps at equal intensity, and hence, the difference between turrets and gaps is much smaller. Therefore, a cloud field having equal amounts of τ-variability in the along-sun and cross-sun directions can be expected to contain stronger along-sun variations, in accordance with the tendency in Figs. 13b and 13c.

A comparison of Figs. 13b and 13c also indicates that the difference between the along-sun and cross-sun directions is larger for CTH than volume extinction coefficient variations. This can be explained by considering that the extra incoming radiation is unattenuated as it reaches the side of turrets in the case of CTH variations, whereas it is attenuated to some degree for VEC variations (Fig. 14b). In addition, for CTH variations, turrets cast shadows even on the top of the gaps,

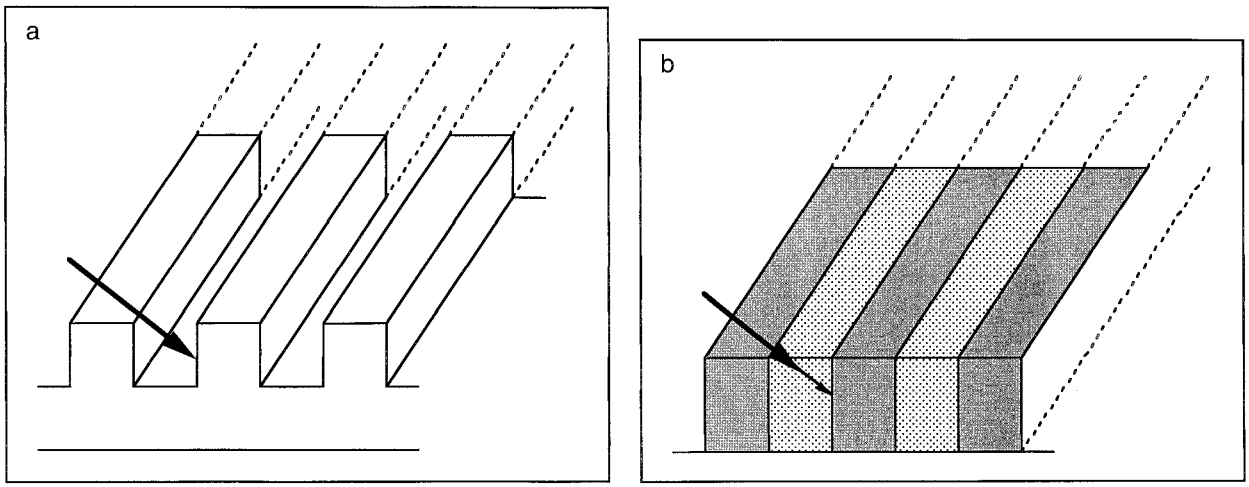

FIG. 14. Turreted stratus cloud geometry: (a) CTH variations and (b) VEC variations. The arrows indicate solar beams reaching the side of turrets.

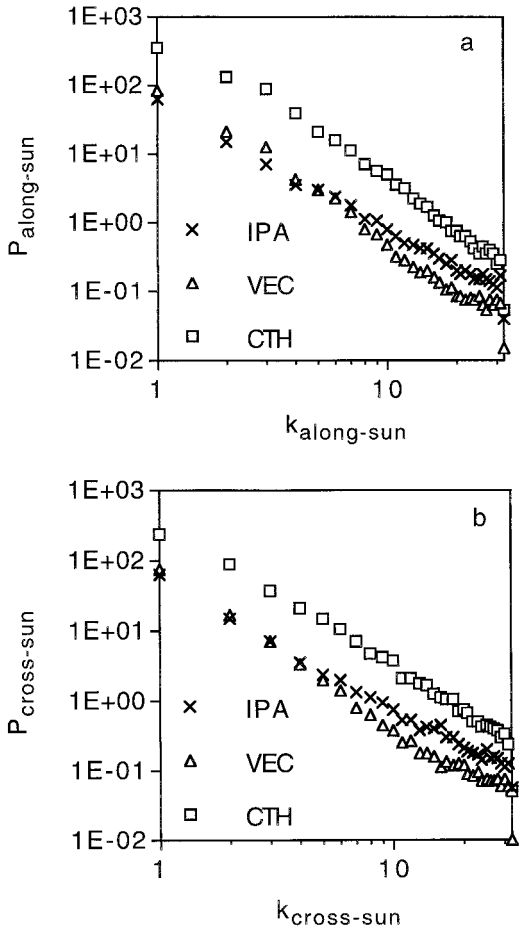

FIG. 15. One-dimensional Fourier spectra of the simulated nadir reflectance fields: (a) along-sun direction and (b) cross-sun direction.

whereas for VEC variations, they reduce only the radiation that enters the thin pixels through their sides.

Many previous studies have examined the one-dimensional Fourier spectrum of satellite images in the directions parallel and perpendicular to the path of the satellite. These spectra were constructed by calculating the one-dimensional spectra separately for each row (or column) and then averaging these spectra over all rows (or columns). Following the same methodology, this paper examines the one-dimensional Fourier spectra in the along-sun and cross-sun directions. Figure 15 shows that, in accordance with the findings of previous studies, for VEC variations, horizontal photon transport smoothes out small-scale variations; that is, $P_{\mathrm{VEC}} < P_{\mathrm{IPA}}$ (P being the Fourier power). At larger scales, however, variations in along-sun direction are enhanced by the sharpening effect: thick pixels receive extra incoming radiation through their sides, whereas thin pixels tend to receive less radiation because they are shadowed by the thicker pixels. The smoothing and sharpening regimes are separated at $k = 5$, which corresponds to a scale of approximately 640 m. This lies between the separation scales of 400 and 800 m seen in Figs. 5 and 6 of Zuidema and Evans (1998). (As discussed in section 3, sharpening influences cloud reflection into various directions to a different degree. As a result, the smoothing and sharpening regimes are separated at $k = 8$, and $k = 1$ in the images of the 50° viewing zenith angle forward and back reflection, respectively.) For CTH variations, the sharpening effect is much stronger and hence dominates at all scales: $P_{\mathrm{CTH}} > P_{\mathrm{IPA}}$.

Since the sharpening effect works mainly in the along-sun direction (a thick pixel casts shadow only on the pixels behind it but not on the ones next to it), cross-sun variations are smoothed out at a larger range of scales in the case of VEC variability; that is, $P_{\mathrm{VEC}} < P_{\mathrm{IPA}}$ for all $k > 3$. The sharpening at larger scales, and

the fact that $P_{CTH} > P_{IPA}$ even for cross-track directions, can be explained by considering that, in moving through the scene in cross-sun direction, one encounters both shadowed and brightened pixels. The fact that along-sun radiative effects also influence cross-sun variability (and vice versa) points out a limitation of using one-dimensional Fourier spectra for examining two-dimensional radiance fields.

5. Influence of cloud and illumination properties

Whereas sections 3 and 4 examined how three-dimensional radiative effects change the appearance of heterogeneous cloud fields, this section discusses how these radiative effects are influenced by cloud and illumination characteristics. In particular, it examines the influence of three factors: the type and magnitude of cloud variability, the average cloud optical thickness, and the solar zenith angle.

For idealized cloud geometries such as cubes or cylinders, it is possible to use simple geometrical considerations to establish quantitative relationships between cloud geometry and radiative properties (e.g., Welch and Wielicki 1984; Schmetz 1984; Bréon 1992). Real clouds, on the other hand, exhibit such a complexity and variety of irregular cloud structures that puts into question whether similar theoretical relationships can be established for them. It would therefore appear more promising to establish such relationships through the statistical analysis of the reflection of numerous heterogeneous cloud fields (Chambers et al. 1997). However, since simulating the reflection of a large number of three-dimensional cloud fields is beyond our current computational capabilities, this paper examines only a limited number of cases to point out some previously unexplored phenomena and draws only qualitative conclusions from the presented numerical results.

Since the sharpening effect works mainly in the along-sun direction, it is convenient to examine the changes in radiative heterogeneity effects through the one-dimensional power spectra of cloud reflection in the along-sun direction. Because it is easier to put the importance of heterogeneity effects into perspective by examining how they change the amplitude (A), rather than the Fourier power (P), of brightness variability at various scales, this section discusses amplitude spectra (calculated as the square root of the Fourier power).

a. Nature and magnitude of cloud variability

Figure 16 shows that radiative processes are very sensitive to the nature of cloud variability. The figure shows not only that the influence of three-dimensional radiative effects is much stronger for cloud-top variability than for extinction coefficient variability, but also that for a wide range of scales ($k > 5$), the two types of cloud variability cause opposite effects to dominate: sharpening for cloud-top variations and smoothing for extinction variations. Since real clouds often have both types of cloud variability, Fig. 16 also displays results for a third cloud field, in which cloud-top and extinction variations have equal influence on the optical thickness variability. This new cloud field has the same optical thickness (τ) distribution, average geometrical thickness, and average VEC as the previously discussed fields, and is constructed in a way that ensures that for any two pixels, the geometrical cloud thickness (z) and extinction coefficient (β) values satisfy the equation

$$\frac{z_1}{z_2} = \frac{\beta_1}{\beta_2} = \left(\frac{\tau_1}{\tau_2}\right)^{0.5}.$$

The results in Fig. 16 indicate that the sharpening effect dominates in the new field. This tendency can be expected since sharpening for cloud-top variability is much stronger than the smoothing for extinction variability.

One could also expect that since, as Fig. 17 shows, the magnitude of cloud-top variability is reduced by about a factor of 2 for the new field (relative to the case of exclusively cloud-top variability), and since the new field also includes extinction variability (for which smoothing dominates over sharpening), the influence of three-dimensional effects should drop to less than half of its value for exclusively cloud-top variability. However, Fig. 16 shows that sharpening drops only about 30%. This discrepancy may be explained by considering that in the new field, cloud-top and extinction variations are well correlated. (The assumption of a close relationship between the two variables is probably not too unrealistic since in many real clouds strong updrafts can cause both bumps in the cloud top and high extinction coefficient values, whereas downdrafts tend to cause both dips in the cloud-top surface and lower extinction coefficient values.) The reason this correlation enhances

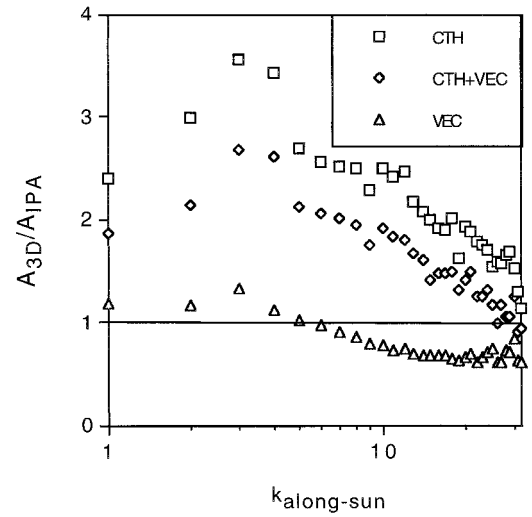

FIG. 16. The influence of three-dimensional radiative effects on the amplitude (A) of along-sun reflectance variations.

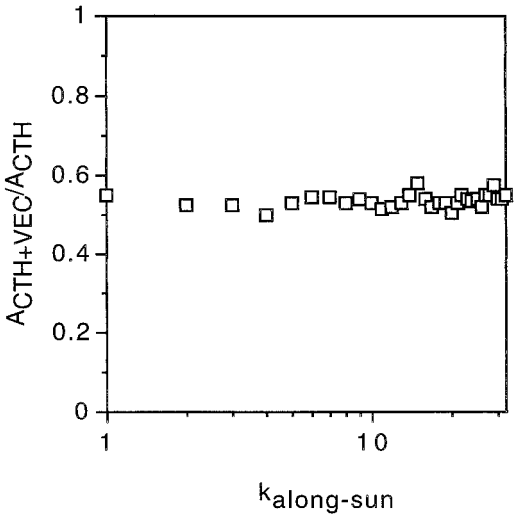

FIG. 17. Ratio of the amplitude of cloud-top variations in two cloud fields.

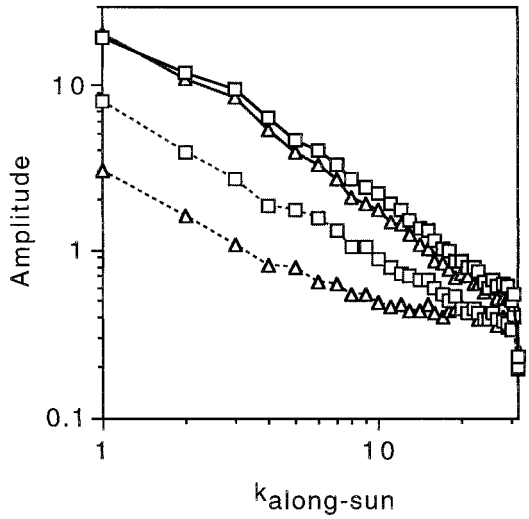

FIG. 18. Amplitude of reflectance variations. Squares and triangles indicate the original and the thick field, respectively. Continuous and dashed lines connect data for CTH variations and for the IPA, respectively.

the sharpening effect is that the new field's cloud bumps tend to be more dense, hence reflecting the extra radiation they receive through their sides more efficiently and casting darker shadows on the areas behind them.

b. Average cloud optical thickness

Davis et al. (1997) show that if the average VEC is kept constant, smoothing becomes more effective with increasing average cloud optical thickness. The enhancement is caused by more multiple scattering, that is, a stronger radiative diffusion in thicker clouds.

As opposed to smoothing, however, sharpening may not be expected to increase significantly with the average optical thickness (if the magnitude of optical thickness variations is kept constant) because it affects mainly direct and low-order scattered radiation, whose amounts are not very sensitive to the average optical thickness. In fact, the brightness variations can be expected to decrease with increasing average optical thickness for two reasons: first, while sharpening remains constant, smoothing becomes more efficient; second, in the IPA, the brightness versus optical thickness curve flattens out at large optical thicknesses (Fig. 4), which implies that identical optical thickness variations cause much smaller brightness variability in thicker clouds.

This expectation is tested by examining how reflection patterns change when the optical thickness of each pixel is increased by 15 (i.e., the cloud geometrical thickness is increased by 500 m). Figure 18 shows that while, as expected, brightness variability drops drastically in the IPA, the drop is much smaller—less than 15%—for CTH variations. The fact that brightness variability does not change much suggests that, as expected, the sharpening effect is not very sensitive to the average optical thickness. It also indicates that cloud properties far from the cloud top (i.e., near the cloud base) do not significantly influence how structured the cloud field appears from above. This implies that the cloud structure that would be observed in a visible satellite image hardly depends on the cloud optical thickness distribution but is mainly determined by cloud variability at or near the cloud top. (Incidentally, in this case, cloud-top variability is correlated with the optical thickness variations.) This argument is also supported by other results presented in this paper (e.g., Fig. 16), which indicate that for a fixed optical thickness distribution, the brightness variability can change by a factor of 3, depending on the magnitude of cloud-top variations.

c. Solar zenith angle

As Zuidema and Evans (1998) show, only the smoothing effect is present for overhead sun. They found that smoothing is much more effective for extinction than for cloud top variations. Figure 19 shows similar behavior at small scales, but at the same time, it indicates that smoothing is stronger for cloud-top variations at larger scales. This scale-dependent behavior may be explained by considering that for CTH variations, radiation scattered out through the side of a thick pixel may not reduce small-scale brightness variations by enhancing the illumination of a nearby, thinner pixel. Instead, it may travel long distances above the cloud top and may reenter the cloud at a point farther away, thereby reducing larger-scale brightness differences. Alternately, if this radiation moves in an oblique upward direction, it may even emerge from the cloud layer unhindered, without brightening any thin pixels. The importance of this second effect (termed ''upward escape'' by Várnai and Davies 1999) is highlighted by the fact that it is also responsible for the enhancement of scene-

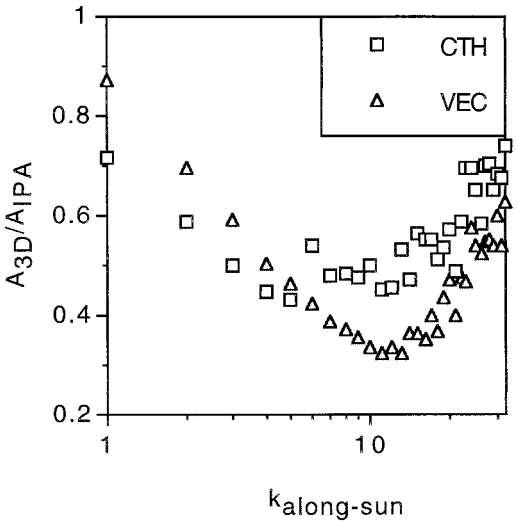

FIG. 19. Influence of three-dimensional effects on the amplitude of reflectance variations for overhead sun.

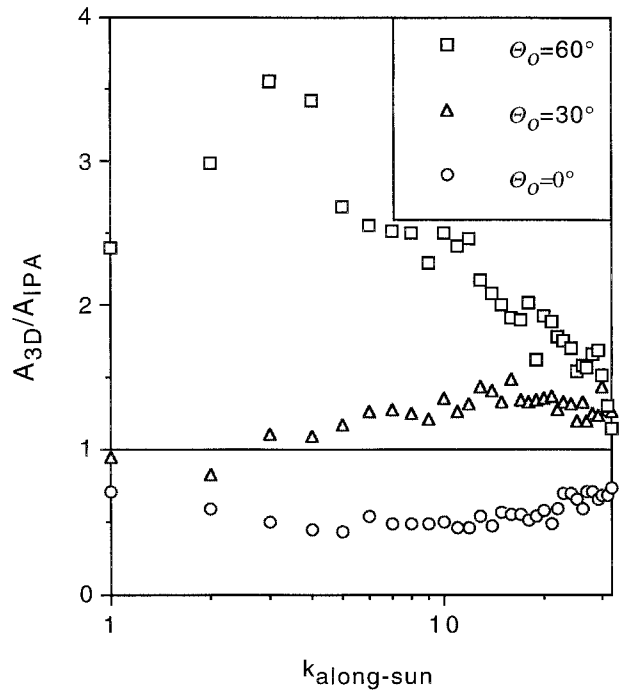

FIG. 20. Influence of three-dimensional effects on the amplitude of reflectance variations for various solar zenith angles.

averaged cloud reflection in oblique directions, described by Davies (1984). It should be noted that in Fig. 19, the reduction in smoothing at the smallest scales is probably due to Monte Carlo simulation errors. These random errors are not significant for the IPA simulation but are comparable to smoothed-out small-scale variations in the three-dimensional fields. Accordingly, the Fourier spectrum of these fields features white noise at the smallest scales.

As the sun moves out from the zenith, direct and low-order scattered radiation tend to move more and more horizontally, and hence the radiative effects that arise from this horizontal movement (i.e., smoothing and sharpening) increase. The increase is most pronounced for the sharpening effect caused by CTH variations, which, as discussed above, can eventually overpower the smoothing effect (Fig. 20). Figure 20 also shows that sharpening first grows at smaller scales and then, as Θ_0 increases, expands to larger and larger scales. (For $\Theta_0 = 30°$, sharpening only extends to ranges $k > 4$, with the maximum at $k \approx 15$, whereas for $\Theta_0 = 60°$, it extends to all examined scales, with its maximum is at $k \approx 3$.) This may be explained by considering that cloud bumps can cast long shadows only for fairly oblique sun: for small solar zenith angles, even large cloud bumps can cast only short shadows.

6. Summary and conclusions

The main purpose of this paper has been to explore the relationship between the spatial distributions of cloud optical thickness (τ) and cloud reflectivity. Since studying this relationship requires extremely lengthy radiative transfer calculations, this paper examined a limited number of cases. As a result, it did not attempt to estimate the radiative influence of cloud heterogeneities on a globally representative distribution of cloud types; instead, its main purpose was to examine some previously unexplored phenomena using a few cases.

Four groups of Monte Carlo radiative transfer simulations were carried out for a scene representative of cumulus clouds having moderate cloud optical thickness variations. The first group of simulations calculated cloud reflection based on the widely used IPA, in which each pixel's reflection is calculated without considering its interactions with neighboring pixels. The second, following most previous studies, assumed flat cloud tops and attributed all τ-variations to horizontal changes in the cloud VEC. Since clouds often do have highly variable tops, the third group of simulations attributed the τ-changes to variations in cloud-top height (CTH) and assumed a constant volume extinction coefficient (VEC). Finally, the fourth type of simulation assumed that CTH and extinction coefficient variations have equal influence on the optical thickness field. In order to make the comparison of the four sets of results most appropriate, all the experiments used the same optical thickness field and the same scene-average CTH and cloud VEC values. The simulations calculated cloud reflection at a 50-m horizontal resolution and generally assumed a 60° solar zenith angle.

This paper examined in detail a phenomenon discovered in previous studies: that cloud reflection at any point is not fully determined by local cloud properties but is also influenced by three-dimensional radiative interactions among nearby cloud elements. As discussed in these studies, two counteracting three-dimensional

effects can occur in heterogeneous clouds that are thick enough to cause significant multiple scattering. First, the smoothing influence of radiative diffusion can reduce the magnitude of brightness variability. Second, for oblique sun, a sharpening effect can enhance the brightness variations: thick pixels appear especially bright because they receive extra solar radiation *through their sides,* while at the same time they make the thin areas behind them especially dark by casting shadows on them. While the smoothing effect is most likely to affect small-scale variability, the sharpening effect can appear at various scales, depending on the cloud structure and the sun view geometry.

This study found that three-dimensional radiative effects—especially sharpening—can change all three first moments (mean, standard deviation, and skewness) of high-resolution reflectance fields. This finding suggests that current high-resolution retrievals of cloud structure from visible satellite images can be significantly biased because they do not take these effects into account. In particular, this study showed that the retrievals significantly overestimate the standard deviation and skewness of the true cloud field and confirmed the finding of Zuidema and Evans (1998) that, although coarse-resolution retrievals using nadir view images underestimate the scene-average optical thickness, high-resolution retrievals tend to overestimate it. The biases were found to be especially large when CTH variations were present: the scene-averaged optical thickness was overestimated by 20% to 60%, depending on the viewing direction, and the standard deviation and skewness values were overestimated to an even larger degree.

Examining the spatial patterns of the simulated reflectance fields revealed that, because the enhancement effect works mainly in directions parallel to the solar azimuth, brightness variations are more intense in these directions than in directions perpendicular to the solar azimuth. This implies that for oblique sun, high-resolution satellite retrievals can result in anisotropies in the retrieved fields that are not present in the true clouds. The retrievals were also found to yield systematically distorted cloud geometries: the sunlit slopes appeared thicker than the shadowy slopes, as if large amounts of cloud water had been moved from the shadowy sides to the sunlit ones.

In addition to examining the influence of three-dimensional radiative effects, this study also discussed how these effects depend on the solar and viewing directions and on various cloud characteristics. It was found that since the sharpening effect grows increasingly stronger as the solar zenith angle increases (thick cloud elements can capture more radiation through their sides and cast longer shadows), three-dimensional radiative interactions have a stronger influence and affect a wider range of spatial scales for more oblique sun. The effects were most pronounced when the scene was viewed from the forward scattering direction, in which case both the shadowed areas and the forward scattering peak of reflection from thick regions were visible. The effects decreased somewhat for nadir view (which is outside the forward scattering peak) and for backscatter view (in which most shadowed areas are hidden from view) but remained significant nonetheless.

The results also revealed that for oblique sun, three-dimensional radiative interactions have much stronger effects for CTH than for VEC variations. These effects are far greater not only on the scene-averaged reflection (as shown in previous studies) but also on the brightness variations of individual pixels. As a result, the correlation between the pixels' optical thicknesses and brightnesses is much weaker when CTH variations are present. When both cloud-top and extinction variations were present and had equal influence on the optical thickness field, the effects of cloud-top variability dominated.

Analyzing the results also indicated that for oblique sun, when CTH variations were present, the observed brightness variations were much more influenced by the sharpening effect caused by the CTH variations than by the optical thickness variations themselves. Since the magnitude of brightness variations depends mainly on cloud properties at or near the cloud top, it was found to be relatively insensitive to parameters that are also influenced by cloud properties at lower levels, such as the scene-average optical thickness.

Overall, the findings indicated that for oblique sun, high-resolution retrievals can introduce large systematic biases into retrieved cloud optical thickness fields, especially if CTH variations are present. Most importantly, the scene-average optical thickness and the magnitude of cloud variability can both be overestimated. In addition, the frequency distribution of the retrieved optical thickness values may be skewed toward large values, the retrieved cloud geometries can be systematically distorted, and artificial anisotropies can be introduced to the structure of the retrieved fields.

Finally, the paper proposed a simple algorithm to determine whether a retrieval based on a satellite image is affected by these biases. The insights presented here may also be helpful in developing new satellite retrieval methods that could take into account the three-dimensional radiative effects.

Acknowledgments. I am very grateful to Laura Atwood, Roger Davies, and Larry Di Girolamo for proofreading the manuscript and providing numerous helpful suggestions. Partial funding for this research from the Jet Propulsion Laboratory of the California Institute of Technology under Contract 959085 is also gratefully acknowledged.

REFERENCES

Barker, H. W., and J. A. Davies, 1992a: Solar radiative fluxes for stochastic, scale-invariant broken cloud fields. *J. Atmos. Sci.,* **49,** 1115–1126.

——, and ——, 1992b: Cumulus cloud radiative properties and the

characteristic of satellite radiance wavenumber spectra. *Remote Sens. Environ.,* **42,** 51–64.

——, and D. Liu, 1995: Inferring optical depth of broken clouds from Landsat data. *J. Climate,* **8,** 2620–2630.

Boers, R., J. D. Spinhirne, and W. D. Hart, 1988: Lidar observations of the fine-scale variability of marine stratocumulus clouds. *J. Appl. Meteor.,* **27,** 797–810.

Bréon, F.-M., 1992: Reflectance of broken cloud fields: Simulation and parameterization. *J. Atmos. Sci.,* **49,** 1221–1232.

Cahalan, R. F., and J. B. Snider, 1989: Marine stratocumulus structure. *Remote Sens. Environ.,* **28,** 95–107.

——, W. Ridgway, W. Wiscombe, S. Gollmer, and Harshvardhan, 1994: Independent pixel and Monte Carlo estimates of stratocumulus albedo. *J. Atmos. Sci.,* **51,** 3776–3790.

Chambers, L. H., B. A. Wielicki, and K. F. Evans, 1997: Accuracy of the independent pixel approximation for satellite estimates of oceanic boundary layer cloud optical depth. *J. Geophys. Res.,* **102,** 1779–1794.

Davies, R., 1976: The three-dimensional transfer of solar radiation in clouds. Ph.D. thesis, University of Wisconsin—Madison, 220 pp. [Available from Memorial Library, University of Wisconsin—Madison, 728 State St., Madison, WI 53706.]

——, 1984: Reflected solar radiances from broken cloud scenes and the interpretation of scanner measurements. *J. Geophys. Res.,* **89,** 1259–1266.

Davis, A., A. Marshak, R. Cahalan, and W. Wiscombe, 1997: The Landsat scale break in stratocumulus as a three-dimensional radiative transfer effect: Implications for cloud remote sensing. *J. Atmos. Sci.,* **54,** 241–260.

Evans, K. F., 1993: Two-dimensional radiative transfer in cloudy atmospheres: The spherical harmonic spatial grid method. *J. Atmos. Sci.,* **50,** 3111–3124.

Gabriel, P. M., S.-C. Tsay, and G. L. Stephens, 1993: A Fourier–Riccati approach to radiative transfer. Part I: Foundations. *J. Atmos. Sci.,* **50,** 3125–3147.

Kobayashi, T., 1993: Effects due to cloud geometry on biases in the cloud albedo derived from radiance measurements. *J. Climate,* **6,** 120–128.

Loeb, N. G., and J. A. Coakley Jr., 1998: Inference of marine stratus cloud optical depths from satellite measurements: Does 1D theory apply? *J. Climate,* **11,** 215–233.

——, T. Várnai, and R. Davies, 1997: Solar zenith angle dependence of solar radiation reflected from inhomogeneous clouds. *J. Geophys. Res.,* **102,** 9387–9395.

——, ——, and D. M. Winker, 1998: Influence of subpixel-scale cloud-top structure on reflectances from overcast stratiform cloud layers. *J. Atmos. Sci.,* **55,** 2960–2973.

Lovejoy, S., D. Schertzer, P. Silas, Y. Tessier, and D. Lavallée, 1993: The unified scaling model of atmospheric dynamics and systematic analysis of scale invariance in cloud radiances. *Ann. Geophys.,* **11,** 119–127.

Marshak, A., A. Davis, W. Wiscombe, and R. Cahalan, 1995a: Radiative smoothing in fractal clouds. *J. Geophys. Res.,* **100** (D), 26 247–26 261.

——, ——, ——, and G. Titov, 1995b: The verisimilitude of the independent pixel approximation used in cloud remote sensing. *Remote Sens. Environ.,* **52,** 71–78.

McKee, T. B., and J. T. Klehr, 1978: Effects of cloud shape on scattered solar radiation. *Mon. Wea. Rev.,* **106,** 399–404.

Pflug, K., and S. Lovejoy, 1993: Differential rotation and cloud texture: Analysis using generalized scale invariance. *J. Atmos. Sci.,* **50,** 538–553.

Schmetz, J., 1984: On the parameterization of the radiative properties of broken clouds. *Tellus,* **36A,** 417–432.

Stephens, G. L., 1988: Radiative transfer through arbitrarily shaped optical media. Part I: A general method of solution. *J. Atmos. Sci.,* **45,** 1818–1836.

Tessier, Y., S. Lovejoy, and D. Schertzer, 1993: Universal multifractals: Theory and observations for rain and clouds. *J. Appl. Meteor.,* **32,** 223–250.

Várnai, T., 1996: Reflection of solar radiation by inhomogeneous clouds. Ph.D. thesis, McGill University, 149 pp. [Available from Bibliographic Services, National Library of Canada, 395 Wellington Street, Ottawa, ON K1A 0N4, Canada.]

——, and R. Davies, 1999: Effects of cloud heterogeneities on shortwave radiation: Comparison of cloud-top variability and internal heterogeneity. *J. Atmos. Sci.,* **56,** 4206–4224.

Welch, R. M., and B. A. Wielicki, 1984: Stratocumulus cloud field reflected fluxes: The effect of cloud shape. *J. Atmos. Sci.,* **41,** 3085–3103.

——, S. K. Cox, and J. M. Davis, 1980: *Solar Radiation and Clouds. Meteor. Monogr.,* No. 39, Amer. Meteor. Soc., 96 pp.

Zuidema, P., and K. F. Evans, 1998: On the validity of the independent pixel approximation for boundary layer clouds observed during ASTEX. *J. Geophys. Res.,* **103,** 6059–6074.